Retinal Models: Comparison of Electronic Absorption Spectra in the Gas Phase and in Methanol Solution

Aurora Muñoz-Losa, Ignacio Fdez. Galván, Manuel A. Aguilar, and M. Elena Martín*

Química Física, Universidad de Extremadura, Avenida de Elvas s/n, 06071 Badajoz, Spain

Received: January 10, 2008; Revised Manuscript Received: April 25, 2008

An accurate study on several models of the 11-*cis*-retinal protonated Schiff base (PSB) has been performed both in vacuo and in methanol solution. Condensed phase calculations have been carried out making use of the ASEP/MD method, which permits the employment of the same high-level ab initio calculations usually applied in gas phase studies as well as a detailed description of the solvent structure around the solute through molecular dynamics simulations of the complete system. The solute structure was completely optimized in vacuo and in solution at the CASSCF level and/or MP2 level, and the CASPT2 method was applied for the calculation of the vertical transition energies and solvent shift values. Our results reproduce and explain the main features of the experimental absorption spectra of the 11-*cis*-retinal PSB. Two well-resolved bands can be identified in vacuo (separated by roughly 1.0 eV), whereas only a single broad band is observed in solution. This fact is explained by the existence of two almost degenerate excited states in methanol. The inclusion of two methyl groups at the iminium end of the system permits the reproduction of the experimental solvent shift value.

Introduction

It is well-known that the interaction of light with the appropriate pigments located in the eye triggers the fascinating visual process. This is possible because these pigments belong to a kind of proteins that permit the interaction between the cell and the environment, which are known as G protein-coupled receptors (GPCRs). Rhodopsin (Rh) is the visual pigment in the rod cells of vertebrates and one of the 700 GPCRs encoded in the human genome. The protein is formed by seven transmembrane helical segments, the opsin, and a polyene prosthetic group called retinal, acting as chromophore. The rhodopsin, responsible for vision under low light intensity conditions (scotopic vision), was the first GPCR whose X-ray crystal structure was available at a 2.8 Å resolution. Although, in general, GPCRs are activated when their agonist occupies the active site, the situation in rhodopsin is slightly different, given that the agonist/antagonist is the very chromophore, covalently attached to the protein through a protonated Schiff base (PSB) linkage to Lys-296. The protein remains inactive (dark state) while the chromophore is in its antagonist form, the 11-cis isomer, and it is activated through the photoinduced isomerization of the chromophore to the all-trans form. Metarhodopsin II (meta II) is the active form of the receptor characterized by an absorption maximum at 380 nm, a band shifted to the blue in ca. 120 nm with respect to the visible absorption maximum characteristic of the dark receptor located at around 500 nm. During the transformation from the inactive to the active form, several intermediate states have been identified in the protein characterized by changes both in the chromophore and in the binding pocket and the whole protein.

Changes in the protein structure alter the interaction between the chromophore and its environment, and these changes cause shifts in the characteristic absorption bands of the chromophore. A quite known case is the one corresponding to the cone cells, responsible for the bright light vision (photopic vision). The pigments present in them contain the same chromophore as rhodopsin, 11-*cis*-retinal, but the binding pockets are different. These differences lead to an absorption maximum located between the near UV (380 nm) and the far visible red (600 nm). Several studies have been dedicated to analyzing the spectral influence of the substitution of one or more amino acids in the protein.[1,2] Changes in the spectra can also be noted when the absorption of the isolated chromophore is compared with the absorption of the chromophore in solution. Without the presence of the protein, which can force particular interactions and hinder others, the chromophore in solution is free to interact in a more profitable way with the solvent molecules. A hypsochromic shift is found for the 11-*cis*-retinal absorption maximum in methanol[3] (442 nm) when compared with its absorption in rhodopsin[4] (≈500 nm). This difference between the transition energy in rhodopsin and that in a solvent is known as the opsin shift. Given that the absorbance at one particular frequency is a consequence of the energy gap between the ground state and the excited state, from the previous result it can be established that the transition is more energetic in methanol, which means that there exists a weaker stabilization of the excited state in solution than in the binding pocket, with respect to the ground state. When compared with the ground state, the first excited state of the 11-*cis*-retinal PSB is characterized by a positive charge transfer from the iminium part to the conjugate chain, so that the charge localization decreases. If the transition energy in solution is compared to the corresponding transition in vacuo, their difference is known as a solvent shift. Since the absorption spectrum of the 11-*cis*-retinal PSB in vacuo is available[5,6] (610 nm), and given its absorption data in different solvents,[3] the solvent shift values can be accurately calculated.

A few studies of 11-*cis*-retinal PSB models in the presence of methanol can be found in the literature. For instance, Gao et al.[7] performed a detailed study of the opsin shift for the bacteriorhodopsin chromophore, performing CIS/3-21 quantum mechanics/molecular mechanics (QM/MM) calculations for the

* Corresponding author. E-mail: memartin@unex.es.

10.1021/jp800244h CCC: $40.75
Published on Web 07/01/2008

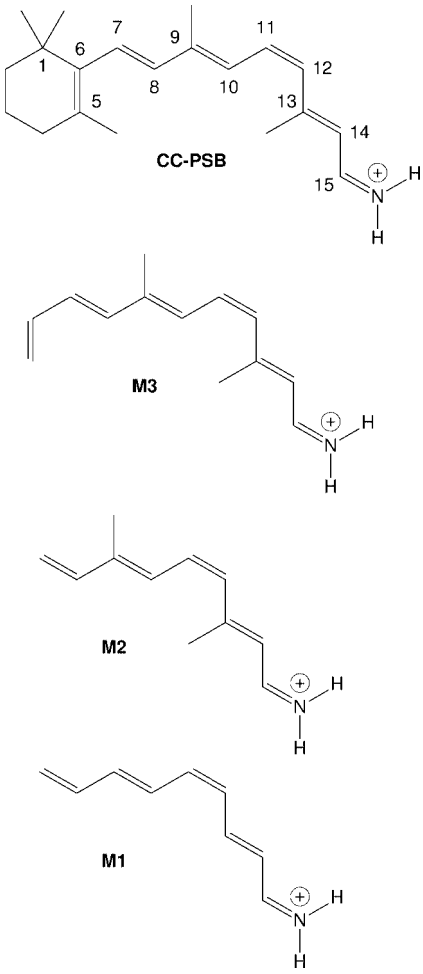

Figure 1. 11-*cis*-Retinal PSB models employed in this study.

study of the chromophore in methanol solution. Andruniów et al.[8] used a higher level of ab initio calculation (CASPT2//CASSCF) to describe the protonated 11-*cis*-retinal Schiff base in the presence of an optimized methanol cluster. Only one solvent configuration is considered, and as a consequence, thermal and entropic contributions are not taken into account.

In a previous article[9] we started the study of the solvent effect on the geometric and spectroscopic characteristics of the 11-*cis*-retinal PSB, making use of the ASEP/MD[10] (averaged solvent electrostatic potential from molecular dynamics data) method. To this end the tEtZtEt-nona-2,4,6,8-tetraenimine cation (M1 in Figure 1) was used as a molecular model to represent the rhodopsin chromophore. On this occasion our aim is to test the validity and the suitability of other, more complex, models for the representation of the main characteristics of the complete chromophore. In particular we will focus in the study of two aspects: (a) the solvent shift magnitude in methanol solution for the vertical absorption transition and (b) the nature of the states responsible for the absorption bands in vacuo and in solution. Apart from the M1 cation, the systems denoted as M2 and M3 (Figure 1) have been considered as qualitative models for the 11-*cis*-retinal PSB.

Molecules with the basic five-double-bond skeleton of M1 have been widely used (see, for instance, refs 11 and 12) as models of the 11-*cis*-retinal PSB because they reproduce important structural features of the real system, such as, for instance, the 11-cis double bond of the chromophore, the iminium residue, and the remaining unsaturated chain with the exception of the β-ionone ring. In our study we have progressively completed the M1 model until reaching the structure of the original chromophore. In this way, when two methyl groups are added to M1, we get the M2 model. The methyl groups do not cause the torsion of the central double bond, and the molecule remains planar. If a sixth double bond is added to the M2 structure, the M3 model is obtained. This double bond simulates the unsaturated bond present in the β-ionone ring, and consequently it makes possible the study of its conjugation effect on the solvent shift magnitude. Besides, its addition causes the torsion of the central double bond of about 9.5°, contrary to the situation in M1 and M2.

The search for reduced molecular models reproducing the structural characteristics of 11-*cis*-retinal PSB and permitting the correct characterization of the main features of its in vacuo and in solution spectra is a consequence of the enormous computational effort necessary to study the complete chromophore. Besides, in the case of the 11-*cis*-retinal PSB, the use of a more reduced system simplifies the study of the processes taking place after the chromophore irradiation as is, for instance, the isomerization path for the excited state through an internal conversion (IC) S_1/S_0. Nevertheless, the continuous improvement of computational resources permits the use of ab initio methods of ever-increasing accuracy for the in vacuo studies on more and more realistic systems. In solution calculations remain much more expensive from a computational point of view because of different factors such as the great number of solvent molecules or degrees of freedom involved. The characterization of the in solution isomerization path for a model of the rhodopsin chromophore using the ASEP/MD method will be the object of a forthcoming paper, whereas in this one we will focus on the first event of the photochemical process, i.e., the vertical transition to the first excited states of the different 11-*cis*-retinal PSB models. In addition, in order to complete our study and with the aim of testing the most accurate computational tools within our reach, we have performed a detailed quantum treatment of the complete chromophore (CC-PSB, in Figure 1) in methanol solution. Although the different isomers of the retinal PSB can interconvert to some extent in solution during preparation and manipulation, the purity of the samples can be mantained to a satisfactory level,[3] such that experimental measuments can be unambiguously assigned to one isomer or other. Consequently, a direct comparison with the experimental data can be made.

Method

Solvent effects on the ground and first two excited states of the above-described systems were dealt with by making use of the ASEP/MD method.[10,13–16] This is a sequential quantum mechanics/molecular mechanics (QM/MM) method, which has demonstrated its utility in the study of many chemical processes, such as conformational equilibrium,[17] absorption and emission electronic spectra,[9,18–20] chemical reactivity,[21] and nonradiative excited-state decay.[22,23]

ASEP/MD can be seen as a QM/MM method implementing the mean field approximation. It combines, alternately, a high-level quantum mechanics (QM) description of the solute system with a molecular mechanics (MM) description of the solvent, one of its main characteristics being the fact that the solvent effect is introduced into the solute wave function in an averaged way. Details of the method have been described in previous papers,[10,13–16] so in this one we will present only a brief outline.

From the two components into which the solvent response is traditionally split, inertial (associated with nuclear movements) and electronic (associated with the response of the electronic

degrees of freedom of the solvent), the latter is considered fast enough to be always in equilibrium with the solute charge distribution. On the contrary, nuclear movements are slower than electrons and longer time periods are needed in order to reach equilibrium. In this context, during a Franck−Condon (FC) transition the change in the solute charge distribution is supposed so fast that the inertial component of the solvent will be in a nonequilibrium situation with the final state; i.e., the solvent structure around the initial state remains fixed during the transition. Consequently, the first step in the study of vertical transitions in solution always consists in the determination of the solvent structure in equilibrium with the solute geometry and charge distribution in the starting state.

In ASEP/MD, as in other QM/MM methods, the solute wave function is obtained by solving the effective Schrödinger equation

$$(\hat{H}_{QM} + \hat{H}^{elect}_{QM/MM} + \hat{H}^{vdw}_{QM/MM})|\Psi\rangle = E|\Psi\rangle \quad (1)$$

where $\hat{H}_{QM}$ is the in vacuo solute molecular Hamiltonian and where now, and this is the distinctive feature of the method, the electrostatic solute−solvent interaction term ($\hat{H}^{elect}_{QM/MM}$) is calculated, using the mean field approximation, as

$$\hat{H}^{elect}_{QM/MM} = \int dr\, \hat{\rho} V_{ASEP}(r) \quad (2)$$

with

$$V_{ASEP}(r) = \langle V_s(r, X)\rangle \quad (3)$$

$V_{ASEP}(r)$ is the average electrostatic potential generated by the solvent and can be represented through a set of point charges $\{q_i\}$. Technical details about the determination of the number, position, and values of the charges can be found in refs 10, 13, and 14. The brackets indicate a statistical average over the configuration space $\{X\}$ obtained in the MD simulation. Finally, $\hat{\rho}$ is the charge density operator of the solute and $\hat{H}^{vdw}_{QM/MM}$ is the Hamiltonian for the van der Waals interaction, often represented by a Lennard-Jones potential.

Given that $V_{ASEP}(r)$ depends on ρ, the solute charge density, eqs 1–3 must be solved iteratively. The process finishes when convergence in the solute charge distribution and energy is reached.

The ASEP/MD method optimizes the solute geometry in the presence of the solvent using a technique described in a previous paper[24] and based on the joint use of the free-energy gradient method[25–27] and the mean field approximation. This technique has been successfully applied to the geometry optimization of ground and excited states of molecules in solution.[9,28] At each step of the optimization procedure the mean value of the total force, $\boldsymbol{F}$, and the Hessian, $\boldsymbol{H}$, of the solute averaged over a representative set of solvent configurations are calculated as the sum of solute and solvent contributions and then used to obtain a new geometry with the Rational Function Optimization method.

Once the optimization is finished, the geometry and charge distribution of the solute initial state and the solvent structure become mutually equilibrated. When one is interested in studying electronic transitions, it becomes necessary to perform an additional self-consistent process during the calculation of the ASEP. The solvent structure and solute geometry obtained in the first self-consistent process are used to couple the quantum mechanical solute and the electron polarization of the solvent. To this end, we assign a molecular polarizability to every solvent molecule, located at its center of mass, and simultaneously replace the effective solvent charge distribution used in the MD calculation by the ab initio gas phase values of the solvent molecule. The dipole moment induced on each solvent molecule is a function of the dipole moments induced on the rest of the molecules and of the solute charge distribution, and hence the electrostatic equation has to be solved self-consistently for each one of the configurations considered. The process finishes when convergence in the solute and solvent charge distributions is reached. During the electron transition we apply the Franck−Condon principle, considering as fixed the solute geometry and the solvent structure around it. However, the electron degrees of freedom of the solvent are allowed to respond to the change in the solute charge distribution.

The total energy of the system (quantum solute + polarizable solvent) is obtained as[9]

$$U = U_{qq} + U_{pq} + U_{pp} + U_{\rho q} + U_{\rho p} + U^{solute}_{dist} + U^{solv}_{dist} \quad (4)$$

Here, q refers to the permanent charges of the solvent molecules, p refers to the solvent-induced dipoles, and ρ is the solute charge density. The last two terms in eq 4 are, respectively, the distortion energy of the solute (the energy spent in polarizing it) and the distortion energy of the solvent (the energy spent in creating the induced dipoles).

By expanding U^{solv}_{dist}, the final expression for the total energy of the system is[20]

$$U = U_{qq} + \frac{1}{2}U_{pq} + U_{\rho q} + \frac{1}{2}U_{\rho p} + U^{solute}_{dist} \quad (5)$$

Once the solvation energy has been calculated for the ground and excited states, the solvent shift can be obtained as the difference:

$$\delta = U_{ex} - U_g = \frac{1}{2}\delta_{pq} + \delta_{\rho q} + \frac{1}{2}\delta_{\rho p} + \delta^{solute}_{dist} \quad (6)$$

The term δ_{qq} cancels out because, in vertical transitions, where the Franck−Condon approximation is applicable, the U_{qq} term takes the same value in both the ground state and the excited state; i.e., the equilibrium solvent structure is only calculated for the ground state. From a practical point of view that means that the first self-consistent process (with or without geometry optimization) is carried out just for the ground state. However, the second cyclic process that permits the response of the electronic degrees of freedom of the solvent is carried out for both the ground and excited states.

Computational Details

The ($\pi \rightarrow \pi^*$) electronic transitions to the first two excited states of a set of different models of the 11-*cis*-retinal PSB have been calculated in vacuo and in methanol solutions. The ASEP/MD method was employed for the in solution calculations. Full ground-state geometry optimizations were performed in both conditions, allowing the total relaxation of all the degrees of freedom at the MP2 and/or CASSCF level of calculation with the split-valence 6-31G* basis set. Nevertheless, the transition energies were always obtained at the CASSCF/6-31G* level of calculation using in each case the complete active π space. That is, for M1 and M2 models the active space used was (10e, 10o), and (12e, 12o) for M3 and CC-PSB. The calculations will be referred to as CASSCF//MP2 and CASSCF//CASSCF for optimizations carried out with MP2 and CASSCF methods, respectively. To improve the energy results, the dynamic electron correlation energy was included with second-order perturbation theory (CASPT2), and consequently, in the same way we mentioned above, these calculations will be referred to as CASPT2//MP2 and CASPT2//CASSCF.

TABLE 1: In Vacuo Intramolecular Parameters for the Different Studied Systems[a]

	CASSCF		MP2				CASSCF		MP2		
distances	M1	M2	M1	M3	CC-PSB	angles	M1	M2	M1	M3	CC-PSB
C_1-C_2					1.54	$C_1C_2C_3$					112.6
C_2-C_3					1.52	$C_2C_3C_4$					108.6
C_3-C_4					1.52	$C_3C_4C_5$					113.2
C_4-C_5					1.51	$C_4C_5C_6$					122.0
$C_5=C_6$				1.35	1.37	$C_5C_6C_7$				124.4	121.9
C_6-C_7				1.46	1.45	$C_6C_7C_8$				124.2	125.3
$C_7=C_8$	1.35	1.35	1.35	1.36	1.39	$C_7C_8C_9$	123.3	125.4	121.9	125.1	124.7
C_8-C_9	1.46	1.47	1.44	1.44	1.43	$C_8C_9C_{10}$	124.2	117.1	124.6	117.0	117.0
$C_9=C_{10}$	1.36	1.36	1.37	1.39	1.39	$C_9C_{10}C_{11}$	120.0	124.8	119.8	124.9	125.0
$C_{10}-C_{11}$	1.45	1.45	1.43	1.42	1.41	$C_{10}C_{11}C_{12}$	128.3	132.7	132.4	130.6	130.5
$C_{11}=C_{12}$	1.36	1.37	1.38	1.39	1.39	$C_{11}C_{12}C_{13}$	125.3	131.2	130.6	130.8	130.7
$C_{12}-C_{13}$	1.44	1.46	1.43	1.42	1.42	$C_{12}C_{13}C_{14}$	123.7	116.3	116.2	116.3	116.5
$C_{13}=C_{14}$	1.36	1.37	1.39	1.40	1.40	$C_{13}C_{14}C_{15}$	120.1	125.3	125.0	125.0	125.1
$C_{14}-C_{15}$	1.42	1.42	1.40	1.39	1.39	$C_{14}C_{15}N$	124.2	121.3	123.5	123.7	123.9
$C_{15}=N$	1.29	1.30	1.32	1.33	1.33						
$C_{13}-C_{16}$		1.51		1.50	1.50						
C_9-C_{17}		1.51		1.50	1.50						
C_5-C_{18}					1.51						
C_1-C_{19}					1.54						
C_1-C_{20}					1.54						

[a] Distances in angstroms and angles in degrees.

CASSCF and MP2 quantum calculations were performed using the Gaussian 98 package of programs.[29] However, it is known that to correctly describe electron transitions in conjugated molecules one must include the dynamic correlation contribution. Hence, once we obtained the solvent structure around the solute, we used the CASPT2 method included in MOLCAS, version 6,[30] to recalculate the transition energies.

As indicated, the ASEP/MD methodology is a sequential QM/MM method that combines in an efficient way the macroscopic description of the solvent structure around the solute through molecular dynamics simulations with a microscopic quantum treatment of the solute properties using accurate ab initio methods. This iterative process of molecular dynamics/quantum calculations was run in all cases for 10 cycles, and the final results were obtained by averaging the last five, when the energy and geometry are converged.

The molecular dynamics (MD) simulations were carried out using the MOLDY program.[31] This program considers the system to be an assembly of rigid molecules, and employs a modification of the Beeman algorithm proposed by Refson.[32] The simulation had one chromophore molecule and 630 methanol molecules at fixed intramolecular geometry confined in a cubic box of 35 Å sides. No counterion was included. Previous studies of Rajamani and Gao[7] and Röhrig et al.[33] using chloride as counterion find that, because of the large dielectric screening effect of methanol, the effect of the counterion on the structure and spectrum of the solute is minimal. This has been corroborated by experiments showing that the position of the chromophore absorption band in polar solvents is not affected by the nature of the counterion.[34] The solute parameters were obtained by combining Lennard-Jones interatomic interactions[35] with electrostatic interactions. Periodic boundary conditions were applied, and spherical cutoffs were used to truncate the solute and methanol interactions at 9 Å. The long-range electrostatic interaction was calculated with the Ewald method.[36] The point charges representing the chromophore molecule during the MD simulation were obtained from the in solution solute molecule wave function by using the CHELPG (Charges from Electrostatic Potential, Grid Method) method.[37,38] The temperature was fixed at 298 K using a Nosé-Hoover[39] thermostat. Each simulation was run for 150 000 time steps, where 50 000 were for equilibration and 100 000 were for production. A time step of 0.5 fs was used. In this way, since the ASEP/MD results are provided by averaging the last five cycles, the average is performed over 250 ps.

Results

As a previous step to the interpretation of the solvent effect on the structure and electronic spectrum of the different studied systems, we will first present the results for the corresponding in vacuo systems. As we mentioned above, geometries were optimized at the MP2 and/or CASSCF level of quantum calculation. In particular, M1 and M2 were optimized using both methodologies and, in accordance with the obtained results, the MP2 method was employed in the geometry optimization of the more complex systems M3 and CC-PSB. Tables 1 and 2 display the most important geometric parameters. The electronic transition energies for all systems were calculated with CASSCF and CASPT2 methods on the optimized geometries.

M1 and M2 show totally planar structures at both MP2 and CASSCF levels, whereas M3 and CC-PSB show twisted geometries in dihedrals C5−C8 and C10−C13. As in similar conjugated polyenes, a clear alternation can be seen between single and double bonds. The bond length alternation (BLA) calculated as the sum of all formal single bond lengths minus the sum of all formal double bond lengths between C7 and C15 is 0.34 and 0.35 Å for M1 and M2 at the CASSCF level and 0.20 and 0.24 Å, respectively, for the calculations at the MP2 level. It can be observed that, on the one hand, CASSCF geometries show a more marked difference between single and double bonds than MP2 ones and besides, the BLA smooths out as the iminium residue is approached. On the other hand, M2 shows greater BLA than M1 at both levels of optimization due to the inclusion of the two methyl groups, which forces the molecule to adopt a conformation that minimizes the interaction with the new sterically hindering groups.

Regarding the M3 and CC-PSB optimized structures in vacuo, they show a C5−C8 dihedral angle of ca. −30° and −41.5°, respectively, and a C10−C13 dihedral angle of −8.5° and

TABLE 2: In Methanol Solution Intramolecular Parameters for the Different Studied Systems[a]

	CASSCF		MP2				CASSCF		MP2		
distances	M1	M2	M1	M3	CC-PSB	angles	M1	M2	M1	M3	CC-PSB
C_1-C_2					1.53	$C_1C_2C_3$					112.5
C_2-C_3					1.52	$C_2C_3C_4$					108.6
C_3-C_4					1.52	$C_3C_4C_5$					113.0
C_4-C_5					1.51	$C_4C_5C_6$					122.3
$C_5=C_6$				1.35	1.36	$C_5C_6C_7$				124.6	122.2
C_6-C_7				1.46	1.47	$C_6C_7C_8$				124.0	125.0
$C_7=C_8$	1.35	1.34	1.35	1.36	1.36	$C_7C_8C_9$	122.5	125.3	122.5	125.3	125.0
C_8-C_9	1.46	1.47	1.45	1.45	1.45	$C_8C_9C_{10}$	126.3	118.1	125.3	117.3	117.4
$C_9=C_{10}$	1.35	1.36	1.36	1.38	1.38	$C_9C_{10}C_{11}$	120.0	124.9	119.0	124.9	125.0
$C_{10}-C_{11}$	1.45	1.45	1.44	1.43	1.43	$C_{10}C_{11}C_{12}$	129.9	131.6	131.9	130.7	130.6
$C_{11}=C_{12}$	1.36	1.36	1.37	1.38	1.37	$C_{11}C_{12}C_{13}$	128.1	132.0	131.0	131.0	131.1
$C_{12}-C_{13}$	1.45	1.46	1.43	1.44	1.44	$C_{12}C_{13}C_{14}$	120.5	115.6	118.1	116.1	116.0
$C_{13}=C_{14}$	1.35	1.36	1.37	1.38	1.38	$C_{13}C_{14}C_{15}$	122.3	124.5	124.6	124.5	124.4
$C_{14}-C_{15}$	1.44	1.43	1.42	1.41	1.41	$C_{14}C_{15}N$	122.5	122.7	122.1	123.2	123.0
$C_{15}=N$	1.28	1.28	1.31	1.31	1.31						
$C_{13}-C_{16}$				1.50	1.50						
C_9-C_{17}				1.50	1.50						
C_5-C_{18}					1.51						
C_1-C_{19}					1.53						
C_1-C_{20}					1.54						

[a] Distances in angstroms and angles in degrees.

−9.5°. We can also observe the same alternation between single and double bonds noted in the planar models M1 and M2. It seems clear that the inclusion of the sixth double bond causes the torsion of the molecule in its central part. With the torsion, the geometric parameters (bond length and angles) from C9 to the iminium extreme become practically coincident for M3 and CC-PSB. Differences are somewhat more evident in the opposite fragment. The trend is clear, when the complete β-ononic ring is introduced: the alternation between single and double bonds decreases, lowering the BLA value (between C5 and C15) from 0.24 Å in M3 to 0.16 Å in CC-PSB.

Vertical transitions have been calculated for each of the described systems to the two lowest excited states. In vacuo, it is common to identify the first and second excited states in PSBs as $1B_u$-like and $2A_g$-like, or ionic state and covalent state, respectively. The calculated transition energies to these states are shown in Table 3. No significant differences have been found between the transition energies for M1 and M2 models; thus the inclusion of the methyl groups has no evident relevance. More interesting changes were evidenced when the sixth double bond or the β-ononic ring was added. The calculations show a decrease in the energy gap from the ground state as the system size increases, reaching values of 2.28 and 1.92 eV for M3 and CC-PSB in their transitions to the first excited state (CASPT2//MP2 calculations). Oscillator strength calculations identify this state as the optically allowed $1B_u$-like state, with f values close to 1. Recently, a photoabsorption experimental study of 11-*cis*-retinal PSB in the gas phase has been published.[6] This study places the absorption band due to the optically allowed excitation to the first electronically excited singlet state at around 2.03 eV (610 nm). Our CASPT2//MP2 calculation for the CC-PSB system is in very good agreement with the experimental data with only a slight deviation (0.10 eV). The small discrepancy with the experimental data can be related to the torsion of the β-ononic ring with respect to the linear chain. This torsion seems to be quite sensitive to the level of calculation as Cembran et al.[40] remarked. These authors found a ca. −68° twist around the C5−C8 dihedral angle, using a CASSCF(12,12) level of optimization and a chromophore similar to CC-PSB. In their study the vertical transition energy to the first excited state was estimated as 2.32 eV. A larger torsion will produce a more important deconjugation of the sixth double bond and consequently an increase of the vertical transition energy. This trend was corroborated by Wanko et al.[41] finding a hypsochromic shift of 0.3 eV when the β-ononic ring of the complete chromophore was forced to a torsion angle of 90° with respect to the original in vacuo torsion of 33° calculated at the B3LYP level.

TABLE 3: Calculated Vertical Transition Energies (eV), Oscillator Strengths, and Solvent Shift Values (eV) for the M1, M2, M3, and CC-PSB Models

	$S_0 \rightarrow$ ionic			$S_0 \rightarrow$ covalent	
	vacuum	solution	δ	vacuum	solution
M1					
CASSCF//CASSCF	3.55	5.22	1.67	4.61	4.62
CASPT2//CASSCF	2.56	3.82	1.26	3.58	3.78
CASPT2//MP2	2.40	3.51	1.11	3.16	3.61
oscillator strength	1.15	1.00		0.09	0.01
M2					
CASSCF//CASSCF	3.34	4.93	1.59	4.34	4.44
CASPT2//CASSCF	2.56	3.68	1.12	3.64	3.45
oscillator strength	0.97	0.87		0.21	0.23
M3					
CASSCF//MP2	3.03	4.08	1.05	4.05	3.78
CASPT2//MP2	2.28	2.99	0.71	3.27	2.88
oscillator strength	0.95	0.91		0.22	0.21
CC-PSB					
CASSCF//MP2	2.54	4.19	1.65	3.42	3.87
CASPT2//MP2	1.93	3.00	1.07	2.77	2.95
oscillator strength	1.20	0.93		0.06	0.15
experimental[6]	2.03	2.76		3.18	

With regard to the calculation level, CASSCF geometries are known to overestimate the BLA, with this factor having a significant influence on the vertical excitation energies. This fact, previously noted by Hufen et al.,[42] can be checked by comparing the calculated transition energies for the M1 model optimized at CASSCF and MP2 levels. For this reason in the rest of our study we have chosen the MP2 method to perform geometry optimizations. Regarding the transition energy values, it seems clear that the inclusion of the dynamic correlation component is compulsory if one wants to obtain accurate results, as CASSCF values are 0.6−1.0 eV higher than CASPT2 values.

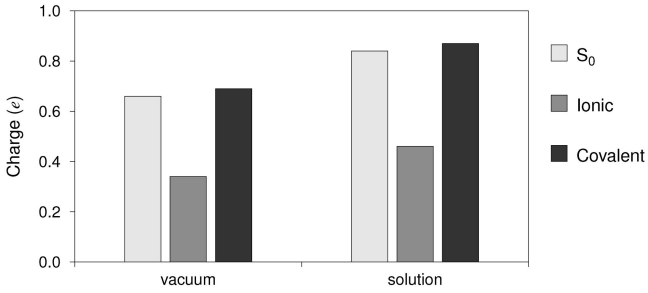

Figure 2. CHELPG charges in vacuo and in methanol solution for the first three singlet states of the CC-PSB model. The structure has been divided in two parts taking the middle point of the $C_{11}-C_{12}$ double bond as reference. The bars represent the total charge of the $C_{12}N$ portion; the remainder of the total $+1e$ charge is distributed in the C_1C_{11} part.

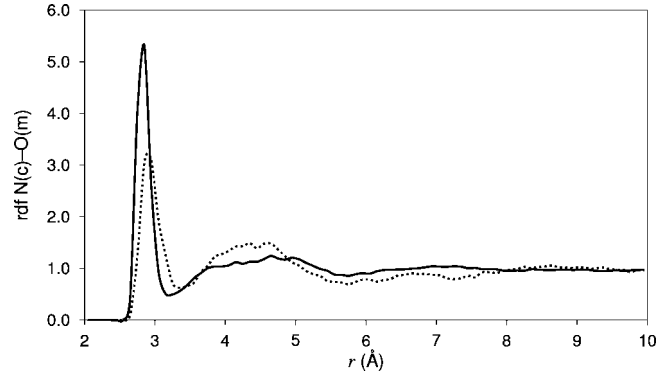

Figure 3. Radial distribution function for the pair formed by the CC-PSB nitrogen atom and the methanol oxygen (N(c)−O(m)). The solid line corresponds to the final averaged radial distribution function, and the dotted line corresponds to the first ASEP/MD cycle function.

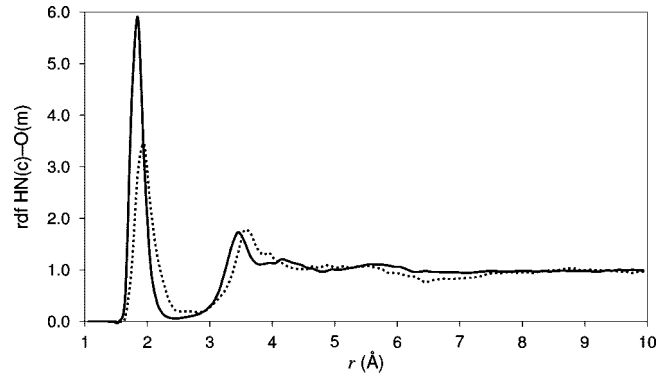

Figure 4. Radial distribution function for the pair formed by the hydrogen linked to the nitrogen atom in CC-PSB and the methanol oxygen (HN(c)−O(m)). The solid line corresponds to the final averaged radial distribution function, and the dotted line corresponds to the first ASEP/MD cycle function.

The second excited state is experimentally estimated to appear just below 400 nm (3.18 eV). This value is again intermediate between the CASPT2//MP2 data obtained for the M3 and CC-PSB systems (3.27 and 2.77 eV, respectively), although it is quite close to both of them. As for the $1B_u$-like state, and in the same ratio, M1 and M2 provide transition energies farther from the experimental data. We can conclude that if one is interested in the reproduction of the electronic transition energies, it is necessary to employ models with at least six double bonds and the inclusion of the dynamic electron correlation. Nevertheless, whatever the model employed in our study the main features of the experimental spectrum are reproduced. That is, in vacuo there exist two well-defined bands, corresponding the more intense to an optically allowed excitation to the first electronic excited singlet state and the other to the so-called "dark" state placed around 1.1 eV higher in the spectrum. From Table 3 it can be noted that the gap between S_1 ($1B_u$) and S_2 ($2A_g$) is always around 1 eV independently of the level of calculation or the model employed.

As mentioned before, the first two excited states in PSBs are normally identified as an ionic state and a covalent state. The oscillator strength reveals that the optically allowed state is the first one. The nature of the different states can be analyzed by taking a look at their electron distributions and wave functions. On the one hand, S_0 and S_2 are two states where there exists an accumulation of positive charge in the iminium end, particularly in the C_{15} and N atoms. Using valence bond terms, as in polyenes, these states correspond to dot−dot or covalent states. On the other hand, S_1 shows a more even distribution of the positive charge along the skeleton, and consequently its nature will be equivalent to a hole-pair (or ionic) excitation. This behavior was analyzed in detail in a previous article for the M1 model.[9] On this occasion we display the charge distribution in the right side of the CC-PSB system (Figure 2). Given the different nature of the states involved in the spectrum, it seems clear that important differences in their charge distributions can be expected. Covalent states display an important accumulation of positive charge close to the iminium end, whereas the ionic state has the charge smoothed along the structure. Similar differences were found by other authors in a system analogous to CC-PSB[40] and the M1 model.[11]

In Solution Study. In this section we will describe and analyze the results obtained in the study of the environmental effects caused by a methanol solution on the structural parameters and vertical transitions for CC-PSB and the M1, M2, and M3 models using the ASEP/MD method. The ground state was optimized in methanol solution, and once the structures of solute and solvent were in equilibrium, the energies of the first three singlet states were calculated with a state average method. Only for the M1 model was the polarizable variant of the ASEP/MD method used and the transition to the ionic state calculated with pure roots.

Solvation causes significant changes in the solute geometry through both specific and bulk interactions. Intramolecular parameters for the different studied systems are displayed in Table 2. As expected, interaction with the solvent produces an increase of the single bond lengths and a decrease of the double bond lengths. This effect is similar in all systems, and more evident in CC-PSB, where the BLA increases 0.2 Å. In solution, the M1 and M2 models remain planar. In the absence of forces driving some specific rotation, any out-of-plane movement is quite improbable. With regard to the M3 and CC-PSB structures, the optimized geometries keep the torsion around the C_6-C_7 and $C_{11}-C_{12}$ bonds; the solvent tends to slightly decrease the torsion in the middle of the skeleton and does not practically affect the disposition of either the sixth double bond or the β-iononic ring.

Another important point is the solvent structure around the solute. For the sake of simplicity we only represent the CC-PSB system in solution: the results found for the rest of the studied models are similar. In Figures 3, 4, and 5 radial distribution functions (rdf's) for the pairs solute nitrogen–methanol oxygen (N(c)−O(m)), hydrogen linked to the solute nitrogen–methanol oxygen (NH(c)−O(m)), and solute nitrogen–hydroxylic hydrogen (N(c)−HO(m)) are displayed. Given the well-defined rdf's, it seems clear that there exists a specific orientation of the methanol molecules around the iminium end.

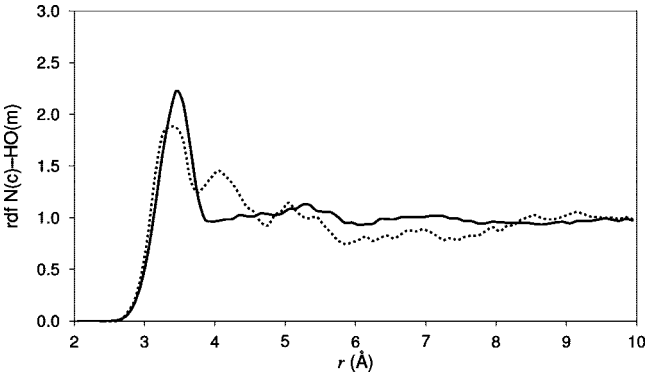

Figure 5. Radial distribution function for the pair formed by the CC-PSB nitrogen atom and the methanol hydroxylic hydrogen (N(c)−HO(m)). The solid line corresponds to the final averaged radial distribution function, and the dotted line corresponds to the first ASEP/MD cycle function.

The first and second solvation shells are visible. The NH(c)−O(m) figure (Figure 4) shows a first peak centered at 1.9 Å indicating the existence of a hydrogen bond. In the N(c)−O(m) rdf (Figure 3) the solvent structure is even more evident. A first peak is clearly located at around 2.9 Å, a second broad solvation shell can be identified between 3.2 and 5.5 Å, and also a third shell could be suspected. Integrating up to the first minimum, a coordination number of 2 is obtained, which is consistent with the formation of two N−H---O hydrogen bonds. Since the N−H bond length is 1.0 Å and the N---O distance is estimated to be 2.9 Å, an almost linear N−H---O disposition of the solute and solvent molecules is deduced. In sum, solute−solvent interaction causes a nonnegligible ordering of the medium. In Figures 3–5, also the rdf of the first cycle of the optimization is displayed. Already at this early stage of the calculation, the solvent shows a clear structure even if as the optimization progresses this structure is more evident, showing a first peak which is higher and slightly displaced to a smaller distance.

Apart from the geometric changes induced by the solvent, the solute−solvent interactions will generate modifications in the solute charge distribution and dipole moment with respect to the in vacuo situation. As expected, the solvent tends to localize the positive charge on the iminium residue. Figure 2 displays the sum of the atomic CHELPG charges on the atoms in the iminium side of the solute molecule, i.e., from the midpoint of the $C_{11}-C_{12}$ bond to the N end. Thus, it shows the extent of the charge localization in this half of the molecule. The ground state and the first two excited states in solution of CC-PSB are displayed. The behavior is completely equivalent in the models M1, M2, and M3. As can be observed, the solvent induces the localization of the positive charge, especially in the covalent states (S_0 and S_2).

Once the solute and solvent structures are known, the calculation of the vertical transition energies in solution is straightforward. Table 3 collects these energies and the corresponding solvent shifts obtained in every case. At the CASSCF level, the interaction with the solvent seems to produce the inversion in the relative position of the first two excited states, with the covalent state becoming lower in energy than the ionic one. The nature of the different states was corroborated by the dominant configuration participating in each state, i.e., doubly excited for the ionic and a HOMO−LUMO transition for the covalent. Oscillator strengths were also calculated; the transition to the upper excited state was the optically allowed transition (*f* value close to 1). The energy difference between the covalent and ionic states varies between 0.68 eV for the M1 model and 0.3 eV for M3 and CC-PSB at the CASSCF//MP2 level of calculation. The scene changes substantially when dynamic correlation is taken into account. Under these conditions, both states become practically degenerate, and we find an energy gap between them of about 0.1 eV. The proximity between these electron transitions means that, contrary to the in vacuo conditions, the theoretical absorption spectrum in solution has two poorly resolved bands, consistent with the possible appearance of a single broad band including the two transitions. Our results confirm the recent experimental study published by Nielsen et al.[6] In this study these authors provide the in vacuo and the in solution electronic absorption spectra of the all-*trans*-*n*-butyl protonated Schiff base in methanol solution and also the in vacuo spectrum for the 11-*cis* dimethyl Schiff base. The in solution recorded spectra for the two isomers are said to be identical. The experimental gas phase spectrum shows a band at 390 nm (3.18 eV) corresponding to the S_2 absorption band maximum and another at 610 nm (2.03 eV) corresponding to the transition to the S_1 state. When the spectrum is recorded in methanol solution, the S_1 band maximum is blue-shifted by more than 150 nm and, what is more important, no resolved S_1 and S_2 bands were found. The spectrum shows only a broad band centered at around 450 nm (2.76 eV). Independently of the model used in the calculations, our theoretical results completely reproduce the appearance of the experimental spectra.

Regarding the reproduction of the absorption maximum in methanol, the theoretical absolute values of the transition energies to the ionic and covalent states decrease, and become closer to the experimental value, as the employed model becomes more similar to the complete chromophore. For M3 and CC-PSB results were practically equivalent and a single band is expected in solution at around 415 nm (3.0 eV) in good agreement with the experiment. On the contrary, the M1 and M2 models provide transition energies blue-shifted by more than 1.50 eV. The utility of these simpler models to simulate the behavior of the complete chromophore lies, more than in the accurate reproduction of the spectroscopic values, in the reproduction of the real system's most important trends. In this context, M1 and M2 have demonstrated their suitability to replicate the peculiarities of both in vacuo and in solution spectra. We will return to this subject in the concluding section.

Another interesting quantity to evaluate is the predicted solvent shift value. These values are also collected in Table 3 and were calculated as the shift suffered by the ionic band as a consequence of the solvent effect. Surprisingly, CASPT2 calculations supply practically the same solvent shift (around 1.1 eV) value independently of the system complexity, except for the M3 model where the value is slightly lower. In all cases the calculated values are larger than the experimental one, estimated as 0.72 eV (2.76 eV, the electronic transition energy in methanol solution,[6] minus 2.03 eV, in vacuo). The fact that the CC-PSB system shows the same solvent shift overestimation as more simplified models (M1 or M2) is due to a structural characteristic of the system shared by all of them. Most of the solvation energy comes from the interaction between the iminium group and the methanol molecules. In all the systems here considered the N atom is bonded to two hydrogen atoms; however, the experiments have been performed with molecules where the N is bonded to $-CH_3$ or more bulky groups. In order to get more details, new calculations were performed. In particular, a new model (M4) was built (Figure 6), replacing the hydrogen atoms linked to the N atom in M1 by two methyl groups. Both CASSCF and MP2 geometry optimizations were performed in vacuo and in methanol solution, keeping the same

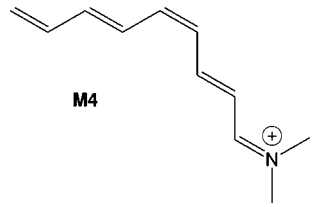

Figure 6. M4 model structure.

conditions as in previous calculations. Important differences can be observed when M4 radial distribution functions are compared to those corresponding to the CC-PSB and M1 systems. The solvent structure around the solute's N atom practically disappears and only a weak and broad peak can be observed at around 4.5 Å for the N(c)−O(m) rdf. No solvent molecules can be assigned to the first solvation shell of the N atom. Less structured solvent around the solute leads to lower solute−solvent interaction energies, especially in the ground state, where the charge is strongly localized, and consequently different energies are expected for the transitions to the excited states. Thus, transition energies to the ionic state were calculated to be 2.69 eV in vacuo and 3.55 eV in solution at the CASPT2//CASSCF level and 2.55 and 3.18 eV at the CASPT2//MP2 level of calculations. These results yield solvent shift values of 0.86 and 0.63 eV at the CASPT2//CASSCF and CASPT2//MP2 levels of calculation, respectively. Comparison with the equivalent results for M1 shows that the incorporation of methyl groups decreases the solvent shift value around 0.4−0.5 eV. This behavior is mainly related, in our opinion, to a decrease of the solvation experienced by the charge localized ground state when hydrogen atoms are replaced by more bulky groups, as two strong hydrogen bonds are lost. If this decrease is directly applied to the CC-PSB solvent shift, the final value becomes 0.65 eV, in very good agreement with experimental data (0.72 eV).

Conclusions

Several models have been tested in order to get an accurate reproduction of the most important features of the electronic absorption spectrum of the 11-*cis*-retinal PSB, chromophore of the membrane protein rhodopsin. Five- and six-double-bond models have been employed. The most important conclusion we would like to note is that any one of them is suitable to display the changes suffered by the experimental in vacuo spectrum when it is registered in methanol solution. From the simpler to the more complex models all of them show transitions to the first two excited states in vacuo with an energy gap between them of around 1.1 eV. Besides, when the study is performed in methanol solution, the transitions to the two states become practically degenerate. This fact explains the appearance in the experimental spectrum of a unique broad band.

At the CASPT2 level of calculation, the solvent shift is well reproduced when methyl group substituents replace the hydrogens linked to the nitrogen atom. Otherwise, a 0.4−0.5 eV overestimation can be found. This fact is related with an excess of solvation due to the presence of hydrogen atoms instead of methyl groups. Even if solvent shift values agree with experimental data, electron transition energies can deviate significantly from the experiment. This happens for the M1 and M2 models, but values tend clearly to the experiment when more complete molecules are employed. As is known, dynamic correlation must be taken into account if one wants to obtain accurate results in conjugated molecules.

In view of the results we can conclude that the simplest M1 model can reproduce, as well as the most complex CC-PSB does, the main features of the absorption electronic spectra of the 11-*cis*-retinal PSB. Its use reduces the required computational cost and could permit the study of postabsorption processes using the most sophisticated quantum methods available. Nevertheless, if one is interested in the reproduction of the experimental transition energies, it seems compulsory to deal with more complex and complete models.

Acknowledgment. This work was supported by the CTQ2004-05680 Project from the Ministerio de Educación y Ciencia of Spain.

References and Notes

(1) McBee, J. K.; Palczewski, K.; Baehr, W.; Pepperberg, D. R. Confronting Complexity: The Interlink of Phototransduction and Retinoid Metabolism in Vertebrate Retina. In *Progress in Retinal and Eye Research*; Elsevier: Oxford, Great Britain, 2001; Vol. 20, p 469.

(2) Nathans, J.; Piantanida, T. P.; Eddy, R. L.; Shows, T. B.; Hogness, D. S. *Science* **1986**, *232*, 203.

(3) Freedman, K. A.; Becker, R. S. *J. Am. Chem. Soc.* **1986**, *108*, 1245.

(4) Wald, G.; Brown, P. K. *Science* **1958**, *127*, 222.

(5) Andersen, L. H.; Nielsen, I. B.; Kristensen, M. B.; El Ghazaly, M. O. A.; Haacke, S.; Nielsen, M. B.; Petersen, M. Å. *J. Am. Chem. Soc.* **2005**, *127*, 12347.

(6) Nielsen, I. B.; Lammich, L.; Andersen, L. H. *Phys. Rev. Lett.* **2006**, *96*, 018304.

(7) Rajamani, R.; Gao, J. *J. Comput. Chem.* **2002**, *23*, 96.

(8) Andruniów, T.; Ferré, N.; Olivucci, M. *Proc. Natl. Acad. Sci. U.S.A.* **2004**, *101*, 17908.

(9) Muñoz Losa, A.; Fdez. Galván, I.; Martín, M. E.; Aguilar, M. A. *J. Phys. Chem. B* **2006**, *110*, 18064.

(10) Fdez. Galván, I.; Sánchez, M. L.; Martín, M. E.; Olivares del Valle, F. J.; Aguilar, M. A. *Comput. Phys. Commun.* **2003**, *155*, 244.

(11) González-Luque, R.; Garavelli, M.; Bernardi, F.; Merchán, M.; Robb, M. A.; Olivucci, M. *Proc. Natl. Acad. Sci. U.S.A.* **2000**, *97*, 9379.

(12) Lee, H. M.; Kim, J.; Kim, C.-J.; Kim, K. S. *J. Chem. Phys.* **2002**, *116*, 6549.

(13) Sánchez, M. L.; Aguilar, M. A.; Olivares del Valle, F. J. *J. Comput. Chem.* **1997**, *18*, 313.

(14) Sánchez, M. L.; Martín, M. E.; Aguilar, M. A.; Olivares del Valle, F. J. *J. Comput. Chem.* **2000**, *21*, 705.

(15) Martín, M. E.; Sánchez, M. L.; Olivares del Valle, F. J.; Aguilar, M. A. *J. Chem. Phys.* **2002**, *116*, 1613.

(16) Sánchez, M. L.; Martín, M. E.; Fdez. Galván, I.; Olivares del Valle, F. J.; Aguilar, M. A. *J. Phys. Chem. B* **2002**, *106*, 4813.

(17) Fdez. Galván, I.; Olivares del Valle, F. J.; Martín, M. E.; Aguilar, M. A. *Theor. Chem. Acc.* **2004**, *111*, 196.

(18) Martín, M. E.; Sánchez, M. L.; Olivares del Valle, F. J.; Aguilar, M. A. *J. Chem. Phys.* **2000**, *113*, 6308.

(19) Martín, M. E.; Sánchez, M. L.; Aguilar, M. A.; Olivares del Valle, F. J. *J. Mol. Struct. (THEOCHEM)* **2001**, *537*, 213.

(20) Martín, M. E.; Muñoz Losa, A.; Fdez. Galván, I.; Aguilar, M. A. *J. Chem. Phys.* **2004**, *121*, 3710.

(21) Fdez. Galván, I.; Aguilar, M. A.; Ruiz-López, M. F. *J. Phys. Chem B* **2005**, *109*, 23024.

(22) Muñoz Losa, A.; Martín, M. E.; Fdez. Galván, I.; Aguilar, M. A. *Chem. Phys. Lett.* **2007**, *443*, 76.

(23) Muñoz Losa, A.; Fdez. Galván, I.; Sánchez, M. L.; Martín, M. E.; Aguilar, M. A. *J. Phys. Chem. B* **2008**, *112*, 877.

(24) Fdez. Galván, I.; Sánchez, M. L.; Martín, M. E.; Olivares del Valle, F. J.; Aguilar, M. A. *J. Chem. Phys.* **2003**, *118*, 255.

(25) Okuyama-Yoshida, N.; Nagaoka, M.; Yamabe, T. *Int. J. Quantum Chem.* **1998**, *70*, 95.

(26) Okuyama-Yoshida, N.; Kataoka, K.; Nagaoka, M.; Yamabe, T. *J. Chem. Phys.* **2000**, *113*, 3519.

(27) Hirao, H.; Nagae, Y.; Nagaoka, M. *Chem. Phys. Lett.* **2001**, *348*, 350.

(28) Muñoz Losa, A.; Fdez. Galván, I.; Aguilar, M. A.; Martín, M. E. *J. Phys. Chem. B* **2007**, *111*, 9864.

(29) Frisch, M. J.; Trucks, G. W.; Schlegel, H. B.; Scuseria, G. E.; Robb, M. A.; Cheeseman, J. R.; Zakrzewski, V. G.; Montgomery, J. A., Jr.; Stratmann, R. E.; Burant, J. C.; Dapprich, S.; Millam, J. M.; Daniels, A. D.; Kudin, K. N.; Strain, M. C.; Farkas, O.; Tomasi, J.; Barone, V.; Cossi, M.; Cammi, R.; Mennucci, B.; Pomelli, C.; Adamo, C.; Clifford, S.; Ochterski, J.; Petersson, G. A.; Ayala, P. Y.; Cui, Q.; Morokuma, K.; Malick, D. K.; Rabuck, A. D.; Raghavachari, K.; Foresman, J. B.; Cioslowski, J.; Ortiz, J. V.; Baboul, A. G.; Stefanov, B. B.; Liu, G.; Liashenko, A.; Piskorz, P.; Komaromi, I.; Gomperts, R.; Martin, R. L.; Fox, D. J.; Keith, T.; Al-Laham, M. A.; Peng, C. Y.; Nanayakkara, A.; Gonzalez, C.; Challacombe, M.; Gill,

P. M. W.; Johnson, B.; Chen, W.; Wong, M. W.; Andres, J. L.; Gonzalez, C.; Head-Gordon, M.; Replogle, E. S.; Pople, J. A. *Gaussian 98*; Gaussian, Inc.: Pittsburgh, PA, 1998.

(30) Andersson, K.; Barysz, M.; Bernhardsson, A.; Blomberg, M. R. A.; Carissan, Y.; Cooper, D. L.; Fülscher, M. P.; Gagliardi, L.; de Graaf, C.; Hess, B. A.; Hagberg, D.; Karlström, G.; Lindh, R.; Malmqvist, P.-Å.; Nakajima, T.; Neogrády, P.; Olsen, J.; Raab, J.; Roos, B. O.; Ryde, U.; Schimmelpfennig, B.; Schütz, M.; Seijo, L.; Serrano-Andrés, L.; Siegbahn, P. E. M.; Stålring, J.; Thorsteinsson, T.; Veryazov, V.; Widmark, P.-O. *MOLCAS*, version 6; University of Lund: Lund, Sweden, 2006.

(31) Refson, K. *Comput. Phys. Commun.* **2000**, *126*, 310.

(32) Refson, K. *Physica* **1985**, *131 B*, 256.

(33) Röhrig, U. F.; Guidoni, L.; Rothlisberger, U. *ChemPhysChem* **2005**, *6*, 1836.

(34) Platz, P. E.; Moheler, J. H. *Biochemistry* **1975**, *14*, 2340.

(35) Cornell, W. D.; Cieplack, P.; Bayly, C. I.; Groud, K. M.; Fergurson, D. M.; Spellmeyer, D. C.; Fox, T.; Cladwell, J. W.; Kollman, P. A. *J. Am. Chem. Soc.* **1995**, *117*, 5179.

(36) Allen, M. P.; Tildesley, D. J. *Computer Simulation of Liquids*; Clarendon Press: Oxford, 1987; p 156.

(37) Chirlian, L. E.; Francl, M. M. *J. Comput. Chem.* **1987**, *8*, 894.

(38) Breneman, C. M.; Wiberg, K. B. *J. Comput. Chem.* **1990**, *11*, 361.

(39) Hoover, W. G. *Phys. Rev. A* **1985**, *31*, 1695.

(40) Cembran, A.; González-Luque, R.; Altoè, P.; Merchán, M.; Bernardi, F.; Olivucci, M.; Garavelli, M. *J. Phys. Chem. A* **2005**, *109*, 6597.

(41) Wanko, M.; Hoffman, M.; Strodel, P.; Koslowski, A.; Thiel, W.; Neese, F.; Frauenheim, T.; Elstner, M. *J. Phys. Chem. B* **2005**, *109*, 3606.

(42) Hufen, J.; Sugihara, M.; Buss, V. *J. Chem. Phys. B* **2004**, *108*, 20419.

JP800244H